

The Convective Urca Process with Implicit Two-Dimensional Hydrodynamics

J. Stein^{1,3} and J.C. Wheeler^{2,4}

ABSTRACT

Consideration of the role of the convective flux in the thermodynamics of the convective Urca neutrino loss process in degenerate, convective, quasi-static, carbon-burning cores shows that the convective Urca process slows down the convective current around the Urca-shell, but, unlike the “thermal” Urca process, does not reduce the entropy or temperature for a given convective volume. Here we demonstrate these effects with two-dimensional numerical hydrodynamical calculations. These two-dimensional implicit hydrodynamics calculations invoke an artificial speeding up of the nuclear and weak rates. They should thus be regarded as indicative, but still qualitative. We find that, compared to a case with no Urca-active nuclei, the case with Urca effects leads to a higher entropy in the convective core because the energy released by nuclear burning is confined to a smaller volume by the effective boundary at the Urca shell. All else being equal, this will tend to accelerate the progression to dynamical runaway. We discuss the open issues regarding the impact of the convective Urca process on the evolution to the “smoldering phase” and then to dynamical runaway.

Subject headings: Physical processes: convection - hydrodynamics - nuclear reactions - Stars: interiors - supernovae

1. Introduction

The nature of degenerate carbon burning prior to runaway in Type Ia supernovae is a long-standing problem that has become more acute with the need to understand the variation

¹Racah Institute of Physics, Hebrew University of Jerusalem, Jerusalem, Israel

²Department of Astronomy, University of Texas at Austin, RLM 15.308, Austin, TX 78712-1083

³E-mail: yossi@phys.huji.ac.il

⁴E-mail: wheel@astro.as.utexas.edu

in the properties of the supernovae that might affect their application to the measurement of cosmological parameters. In this context, it is important to determine the effect of the convective Urca process because it may have direct observational implications for Type Ia supernovae. The convective Urca process can affect the density at which carbon undergoes dynamic runaway, subsequent electron capture and neutronizing reactions in the explosion, the size and gradient in the carbon/oxygen ratio at runaway, and the spectrum of convective motions and hence subsequent Rayleigh-Taylor unstable dynamic burning.

The essence of the convective Urca process was first presented by Paczyński (1972) whereby the convective circulation driven by carbon burning in degenerate white dwarfs will yield first electron capture and then β -decay of susceptible nuclei. This yields no net change in composition, but a loss of neutrinos (or antineutrinos) at each step of the cycle along with their attendant energy. Paczyński argued that this cycle would cool the star and postpone dynamical runaway. Previously, it had been pointed out by Bisnovatyi-Kogan & Seidov (1970) that non-equilibrium weak interactions as involved in this process would yield local heating. Bruenn (1973) independently pointed out that each weak interaction added heat to the system, despite the loss of the neutrino. As electrons are captured below the Fermi sea, another electron will drop from the Fermi surface to fill the “hole,” resulting in heat. In the other portion of the cycle, β -decay will deposit electrons with excess thermal energy above the Fermi sea. Paczyński (1974) acknowledged the arguments of Bisnovatyi-Kogan & Seidov and of Bruenn and pointed out that the energy flow between carbon burning and Urca neutrinos depends on the interaction between the convective and Urca processes. He noted that evolutionary calculations by Couch & Arnett (1973) and by Ergma & Paczyński (1974) were done with the implicit assumption that Urca neutrinos directly remove heat from the stellar interior. In this paper Paczyński also noted that the convective Urca process will lead to a gradient in the electron abundance.

The physics of the convective Urca process was analyzed by Barkat & Wheeler (1990; hereafter BW), who argued that convective currents of composition play a critical role in the quasi-steady state thermodynamics of the convective Urca process, so that cooling terms associated with the convective flow exactly cancel the microscopic heating terms described by Bruenn and lead to net cooling. Their results seemed to be consistent with the results of the careful numerical work of Iben (1978a,b, 1982).

The conclusions of BW were called into question by Mochkovitch (1996). Mochkovitch presented a general thermodynamic analysis and concluded that the convective Urca process must heat the star. These issues were addressed again by Stein, Barkat & Wheeler (1999; hereafter SBW) who concluded, in agreement with Mochkovitch, that while the neutrinos associated with the convective Urca process carry away energy, the entropy, and the temper-

ature, cannot decline. BW included a “work” term that effectively removed energy from the total energy budget that could only have come from the kinetic energy, which must remain positive. The loss rate by the Urca process cannot exceed the rate of generation of kinetic energy. Rather, the convective Urca neutrino losses slow the convective currents (SBW, Bisnovatyi-Kogan 2001; Lesaffre, Podsiadlowski & Tout 2005).

Here we present calculations demonstrating the role of the convective Urca process in two-dimensional simulations and illustrate that the conclusions of SBW were correct. In particular, we examine the role of convective currents, buoyancy and mixing in creating and limiting the kinetic energy.

We present the outline of the input physics in §2 and the numerical technique in §3. The results are presented in §4 and conclusions are presented in §5.

2. Description of Physics and Models

2.1. Initial setting

We constructed a Carbon-Oxygen core ($1.38M_{\odot}$) with equal abundance of C and O by mass and with $\rho_c = 3.5 \times 10^9 \text{ g cm}^{-3}$ and $T_c = 3 \times 10^8 \text{ K}$ in which the inner region ($0.79M_{\odot}$) had constant entropy, and the outer region was isothermal. For the $^{23}\text{Ne}/^{23}\text{Na}$ Urca pair, the Urca shell is at a density of $1.7 \times 10^9 \text{ g cm}^{-3}$. In these calculations, the Urca shell falls in the middle of the constant-entropy region, and divided that region into an inner zone ($0.31M_{\odot}$) and an outer zone. This setup was necessary to distinguish the effects of the Urca process on the convection from the effect of the steep entropy gradient in the isothermal part. The inner zone contained a small concentration ($0.00004 - 0.0004\%$) of “mother” Urca nuclei (^{23}Ne) and the outer zone with the rest of the star contained the same concentration of “daughter” Urca nuclei (^{23}Na). This division between the inner and outer zones is stable against convection, even without the Urca process, as long as the entropy of the outer zone is equal to (or even very slightly less than) the entropy of the inner zone. In order to see the stabilizing effect of the Urca process on the convection we had to create a marginally stable configuration. We achieved this by slightly reducing the entropy of the outer zone, and creating a slightly *unstable* configuration. This instability triggered a violent convection, which settled down after a short time, leaving the simulation in the desired configuration.

2.2. Reaction rates

For the Carbon burning we used a simplified reaction rate which turns Carbon into Oxygen:

$$\frac{dX_c}{dt} = -0.5775 X_C^2 (\rho_9)^{2.79} (T_9)^{22} \quad (1)$$

where ρ_9 is the density in units of 10^9 g cm^{-3} and T_9 is the temperature in units of 10^9 K . The q-value for the reaction is $q = 2.857 \times 10^{17} \text{ erg gm}^{-1}$. The Urca data for density thresholds and rates were taken from Ergma and Paczyński (1974). In order to distinguish between the convective Urca process and the cooling thermal Urca process, we neglect the thermal Urca process. Other neutrino losses were taken from Itoh and Kohyama (1983). In our simulations we multiplied all the rates by factors 2000 or 20000 in order to speed up the process. Even so, the simulations required hundreds of thousands time-steps to produce $\sim 10^4$ seconds of simulation “star time.”

3. Numerical Procedure

The goal of this program is to simulate convection in a marginally stable carbon-oxygen core, where the sound-speed is high and the material velocity is low. Two-dimensional simulation of subsonic convection in the central part of a white-dwarf presents some major stability problems:

1. Having nearly the Chandrasekar mass, the star is only marginally stable to small perturbations.
2. Convection occurs in a region with huge density and temperature gradients, but almost constant entropy. The convection is driven by the tiny entropy gradients. Small density or temperature fluctuations caused by numerical inaccuracies may create large entropy gradients, destabilizing the convection.
3. The velocities are subsonic, so $\nabla \cdot (\rho \mathbf{u})$ is almost zero, in spite of the large density gradients.

These issues consequently require a very stable numerical procedure. In order to address these stability issues, we therefore incorporated the following features into our program entitled DWARF:

1. We use an implicit Eulerian scheme with second-order donor.
2. In order to avoid the “chessboard black-white” decoupling of the cells in a usual staggered mesh, where density, energy and pressure are defined inside the cells and the velocity is defined on the corners, we define the velocities on the edge-centers of the 2D cells.
3. Since the pressure differences between adjacent cells due to density differences may be larger by several orders of magnitude than the pressure difference due to the entropy differ-

ences, we take special care that the advection terms will not create spurious large entropy gradients.

3.1. Hydrodynamic equations

The hydrodynamic equations are:

Acceleration:

$$\frac{\partial \mathbf{u}}{\partial t} = -\frac{1}{\rho} \nabla p - (\mathbf{u} \cdot \nabla) \mathbf{u} - \mathbf{G} \quad (2)$$

Mass conservation:

$$\frac{\partial \rho}{\partial t} = -\nabla \cdot (\rho \mathbf{u}) \quad (3)$$

Internal energy:

$$\frac{\partial e}{\partial t} = -\nabla \cdot (e \mathbf{u}) - p \nabla \cdot \mathbf{u} + q \quad (4)$$

where \mathbf{u} is the velocity, ρ is the density, e is the energy per unit mass, \mathbf{G} is the gravitational force and q is the energy source per unit mass per unit time. We use spherical coordinates, r, θ, ϕ , and assume that the gravity has spherical symmetry. All other quantities are treated in cylindrical symmetry.

In these coordinates and under these assumptions our equations become:

Acceleration:

$$\frac{\partial u_r}{\partial t} = -\frac{1}{\rho} \frac{\partial p}{\partial r} - g_r - u_r \frac{\partial u_r}{\partial r} - \frac{u_\theta}{r} \frac{\partial u_r}{\partial \theta} + \frac{1}{r} u_\theta^2 \quad (5)$$

$$\frac{\partial u_\theta}{\partial t} = -\frac{1}{\rho r} \frac{\partial p}{\partial \theta} - \frac{u_\theta}{r} \frac{\partial u_\theta}{\partial \theta} - u_r \frac{\partial u_\theta}{\partial r} - \frac{1}{r} u_r u_\theta \quad (6)$$

Mass:

$$\frac{\partial \rho}{\partial t} = -\frac{1}{r^2} \frac{\partial (r^2 \rho u_r)}{\partial r} - \frac{1}{r \sin \theta} \frac{\partial (\rho u_\theta \sin \theta)}{\partial \theta} \quad (7)$$

Energy:

$$\frac{\partial \rho e}{\partial t} = -\frac{1}{r^2} \frac{\partial (r^2 \rho e u_r)}{\partial r} - \frac{1}{r \sin \theta} \frac{\partial (\rho e u_\theta \sin \theta)}{\partial \theta} \quad (8)$$

We set rigid boundaries in angle at $\theta = 45^\circ$ and at 135° and in mass at an inner boundary of $10^{-4} M_\odot$ and an outer boundary of $1.38 M_\odot$. The two angle and inner mass boundaries were chosen to avoid the singularity of spherical coordinates. The outer mass boundary was adopted for stability reasons. Despite the latter rigid outer boundary, the radial relaxation (expansion) of the convective region was not affected.

3.2. Features of the Program DWARF

The DWARF code incorporates a rectangular grid in polar coordinates. It uses a staggered-mesh with implicit-pressure scheme, in which only the pressure is treated implicitly (See Livne 1993 and references therein), is adequate for subsonic flow in an otherwise stable medium. In our particular case, this model shows strong Chessboard black-white decoupling of the cells, causing diagonal instability. This decoupling is caused by the fact that in this model $\frac{\partial P_{i,j}}{\partial P_{k,l}}$ is nearly zero, when $(k, l) = (i, j \pm 1)$ or $(k, l) = (i \pm 1, j)$. To avoid this instability we chose a different staggered-mesh, in which the velocities and accelerations are defined at edge-centers. Other physical quantities are defined at the cell-centers. For the implicit-pressure scheme, (see Livne 1993 and references therein), only the $M_{ij,kl} = \delta_{i,k}\delta_{j,l} - \frac{\partial P_{i,j}}{\partial P_{k,l}}$ matrix is inverted; however, this derivative accounts for both acceleration and advection.

To compute the acceleration, we divide the acceleration into two parts:

- 1- Direct accelerations, $\frac{1}{\rho} \frac{\partial P}{\partial r} - g_r - u_r \frac{\partial u_r}{\partial r}$ and $\frac{1}{r\rho} \frac{\partial P}{\partial \theta} - \frac{u_\theta}{r} \frac{\partial u_\theta}{\partial \theta}$, are treated implicitly.
- 2- Centrifugal ($\frac{1}{r} u_\theta^2$) and Coriolis ($-\frac{1}{r} u_r u_\theta$) accelerations are treated explicitly, using the values at the end of the time-step.

Stability requires that the advection be computed by a donor scheme; however, a donor scheme is difficult to treat implicitly, because the dependence of the advection on the velocity has discontinuous derivatives. Therefore we divided the advection into two parts:

- 1- Using centered values (no donor) in the implicit part.
- 2- Correction to a second order donor scheme is done explicitly.

Choosing the “centered” donor can be done in several ways. Since the convection is driven by entropy gradients, we defined “centered” to be average density, entropy and composition of the two adjacent cells. The energy and temperature were calculated from these values by using the equation of state.

4. Results

We present the results of 5 simulations:¹

- S-4-2E4-0: ($X_{Ne} = 4 \times 10^{-4}$), reaction-rates multiplied by 20000, Urca-rate = 0.
- S-4-2E4: ($X_{Ne} = 4 \times 10^{-4}$), reaction-rates multiplied by 20000, Urca-rate multiplied by 2000.
- S-1-2E4: ($X_{Ne} = 1 \times 10^{-4}$), reaction-rates multiplied by 20000, Urca-rate multiplied by 2000.
- S-0.4-2E4: ($X_{Ne} = 4 \times 10^{-5}$), reaction-rates multiplied by 20000, Urca-rate multiplied by 2000.

¹computational models HN, FH, GG, EG and FI, respectively

S-4-2E3: ($X_{Ne} = 4 \times 10^{-4}$), reaction-rates multiplied by 2000, Urca-rate multiplied by 2000. When we multiplied the Urca-rate by another factor of 10 (to 20,000), the results did not change significantly, although the Urca-gradients became steeper, spreading over fewer cells. We thus left Urca rate multiplication factor at 2000 for all models where Urca effects were incorporated.

All simulations were computed a long time after the convection settled down. Simulations S-4-2E4, S-1-2E4 and S-0.4-2E4 (varying the Urca abundance) ran up to 6000 simulation-time seconds. Simulation S-4-2E4-0 (with no Urca) ran up to 10,000 simulation-time seconds and simulation S-4-2E3 (with reduced nuclear rate acceleration), which was slower than the rest, ran up to 20,000 simulation-time seconds. The velocity scale in all the 2D figures (3 - 6 below) is normalized so that a single horizontal tic mark corresponds to a velocity of 10 km s^{-1} . For the online color figures the velocity is as follows: black arrows: below 10^5 cm s^{-1} ; red arrows: $10^5 - 2 \times 10^5 \text{ cm s}^{-1}$; green arrows: $2 \times 10^5 - 4 \times 10^5 \text{ cm s}^{-1}$; blue arrows: $4 \times 10^5 - 8 \times 10^5 \text{ cm s}^{-1}$.

The energy input by nuclear reactions is converted in part to the kinetic energy of the convective circulation. The fraction of the input energy that ends up in kinetic energy depends on the dissipation to Urca “viscosity,” to turbulent viscosity and, for simulations, into numerical viscosity. For reference, the total energy input rate for simulation S-4-2E4 is $2 \times 10^{42} \text{ erg s}^{-1}$. The Urca neutrino loss rate is about $10^{41} \text{ erg s}^{-1}$. The total Urca dissipation rate including heating is about $1.3 \times 10^{41} \text{ erg s}^{-1}$, about 6.5 percent of the energy input. As shown in SBW, the rate of conversion of thermal energy to kinetic energy up to the Urca shell ($T \sim 1.9 \times 10^8 \text{ K}$) is less than $(T_c - T_U)/T_c \sim 37$ percent, where T_c is the central temperature and T_U is the temperature at the Urca shell. This implies that the Urca process as computed here makes a significant contribution to the kinetic energy dissipation in terms of the estimated maximum dissipation.

Figure 1 shows the kinetic energy of all the simulations. In simulations S-4-2E4, S-1-2E4, and S-0.4-2E4 in which the nuclear rates were all multiplied by 20,000, but the abundance of Urca nuclei varied by a factor of 10, the kinetic energy associated with the convection settled rapidly into a quasi-steady state after recovering from the initial instability. In simulation S-4-2E4-0, which had no Urca effect, the convection spread to fill the whole inner, constant entropy region, and so the approach to steady state took longer. Simulation S-4-2E3, with the nuclear rate enhanced by only a factor of 2000, took much longer to reach steady state. Simulations S-4-2E4, S-1-2E4, and S-0.4-2E4 converged to more or less the same kinetic energy, showing that in these simulations the kinetic energy does not depend sensitively on the abundance of the Urca nuclei, as long as the Urca physics is active. Simulation S-4-2E4-0, which lost no kinetic energy to the Urca effect, reached a somewhat higher value of kinetic

energy. Simulation S-4-2E3, with a nuclear rate 10 times less asymptoted to a value around 4 times smaller than simulations S-4-2E4, S-1-2E4, and S-0.4-2E4. This gives some notion of the dependence of the convective kinetic energy on the rate of nuclear energy input.

Figure 2 shows the total Urca neutrino loss rate of all the simulations. Although there are large fluctuations, the general trend is that a higher abundance of Urca nuclei leads to *smaller* neutrino losses. Specifically, simulation S-4-2E4, which had the highest concentration of Urca atoms, lost *less* energy to Urca neutrinos by a factor of 2 to 3 than simulations S-1-2E4 and S-0.4-2E4. This is presumably related to the fact that the higher ^{23}Ne abundance restricted the extension of the convection beyond the Urca shell and the attendant mixing outward of carbon-burning products compared to simulations with small abundances of Urca-active nuclei (see Figures 3 below). On the other hand, we cannot rule out that this difference is affected by our numerical resolution. Simulation S-4-2E3, which had the smallest nuclear rate enhancement lost less energy to the Urca neutrinos than simulation S-4-2E4, by a factor of about 5, which is very similar to the ratio of a factor of 4 between the asymptotic kinetic energies of the two simulations. This suggests that the Urca neutrino loss rates are roughly proportional to the kinetic energy in the regime where Urca losses control the extent of convection (see the Appendix for a discussion of conditions where strong convection may overwhelm the Urca process).

The question this work was designed to address is: “What does the Urca effect do?” The answer to this question, our main result, is presented in Figure 3. These figures show the percentage of burned carbon (more accurately: $0.5 - X_C$), for simulations S-4-2E4-0, S-4-2E4, S-1-2E4, and S-0.4-2E4 respectively. The carbon burns near the center. When no Urca effect is present - the convective currents spread the carbon-burning products evenly over the whole inner region (Figure 3A, simulation S-4-2E4-0). In Figure 3B, simulation S-4-2E4, only a small percentage of the carbon-burning products sneaks through the Urca-shell. This percentage increased as X_{Ne} was decreased (Figures 3C and 3D).

Figure 4 shows the entropy in simulations S-4-2E4-0 and S-4-2E4, respectively. Note the decrease of the entropy beyond the Urca-shell in simulation S-4-2E4, which compensates for the increase in the number of electrons per atom.

Figure 5 shows the abundance of Urca-active Ne^{23} atoms in the inner region of simulations S-4-2E4-0 and S-4-2E4, respectively. As expected, in simulation S-4-2E4-0 the abundance is homogeneous, while in simulation S-4-2E4, the Ne^{23} abundance is 0.0004 inside the inner zone within the Urca shell, and zero in the outer zone beyond the Urca shell, except for a narrow transition zone near the Urca-shell. Figure 6 shows the Urca neutrino loss-rate in simulation S-4-2E4. The whole Urca activity occurs near the Urca-shell, with the exception of some boundary-related activity. In all the 2D figures, the overshootings at

the left and right boundaries are numerical artifacts.

5. Conclusions

These two-dimensional calculations make no assumptions about the convective Urca process *per se*; they employ the relevant weak interaction microphysics and then follow the affects of the convective flow with no extra assumptions about thermal or chemical equilibrium. Work done by convection and associated neutrino losses are computed straightforwardly. Because the computations have been done with artificially accelerated thermonuclear and weak interaction rates, they cannot be taken literally; some processes like turbulent dissipation will not scale linearly with these rates. It would, of course, be desirable to do these simulations in three, rather than two dimensions. We expect the qualitative results to be the same, but this must eventually be checked. Our results should therefore be judged for their qualitative value.

With these caveats, we conclude here: a) In agreement with Mochkovitch (1996) and SBW and in disagreement with the earlier work in BW, that the convective Urca process cannot result in a net decrease in entropy, and hence in temperature, for a constant or increasing density; b) that the Urca process controls the convective flow and affects the kinetic energy even as the convective motions drive the Urca process; c) that the convective Urca process will, at least temporarily, limit the expansion of the convective zone beyond the Urca shell. Bisnovatyi-Kogan (2001) also noted that the convective Urca process must slow the speed of convection. Despite their qualitative nature, we feel these simulations have established that *the convective Urca process is fed by the positive definite kinetic energy and cannot cool the star, but can and will affect the nature of the convective flow*.

Over the last couple of decades most work on modeling of the progenitors of Type Ia supernovae has simply ignored the effects of the convective Urca process. It remains to be seen whether the convective Urca process will have a significant effect on the ultimate dynamical runaway. The convective Urca process by itself will not lead to dynamical runaway at higher density because it cools the star, as hypothesized in some earlier work. The convective Urca process may shorten the “smoldering” phase (Höflich & Stein 2002) between carbon ignition, defined as the epoch when carbon burning exceeds neutrino losses, and dynamic runaway. Compared to a model without the effect of the convective Urca process, the convective core, and hence the heat liberated by the carbon burning, is confined to a smaller volume. All else being equal, a model that invokes the convective Urca process should proceed to dynamical runaway more quickly than one without the convective Urca process. The net result might be to indirectly lead to dynamic runaway at lower density with effects

on the explosion dynamics, nucleosynthesis, and light curve.

These issues will depend sensitively on whether there is an active Urca shell and that, in turn, depends on the density of carbon ignition. While that issue was once actively explored, it has received little commentary in recent literature on the topic of degenerate carbon burning. This is in part due to advances in understanding of weak interaction rates (see Brachwitz et al. 2000, and references therein) and partly due to settling on a standard set of assumptions for the treatment of effects such as plasmon neutrino losses and strong screening effects (that may or may not be correct).

Calculations of non-rotating accreting white dwarf evolution tend to give carbon ignition at densities exceeding $4 \times 10^9 \text{ gm cm}^{-3}$ for modest accretion rates, $\sim 10^{-9} \text{ M}_\odot \text{yr}^{-1}$, depending on the mass of the original white dwarf and the temperature at the beginning of the accretion phase (Bravo et al. 1996; Höflich, Nomoto, Umeda & Wheeler 2000). Lesaffre et al. (2006) estimate the distribution of central densities for single-degenerate progenitors and find a broad distribution with a minimum ignition density of $\sim 2 \times 10^9 \text{ g cm}^{-3}$, above the threshold density for the Ne/Na Urca pair. Such conditions will inevitably be accompanied by one or more convective Urca shells. These conditions might be expected to lead to nova outbursts that prevent growth to runaway. If growth of the white dwarf continues, the result could be accretion-induced collapse (Saio & Nomoto 1998). It will be interesting to investigate whether or not confinement of convection to Urca shells and the subsequent tendency to heat a smaller volume more rapidly would affect this conclusion. Only for rather high accretion rates, approaching $10^{-6} \text{ M}_\odot \text{yr}^{-1}$, will the central density at carbon ignition be less than the threshold density for the Ne/Na convective Urca cycle so that the convective Urca process might not occur at all. For these high rates, there is some danger of excessively polluting the circumstellar environment with a hydrogen-rich wind.

Observational constraints on Type Ia supernovae tend to put the central density at ignition in a range where the Urca process might occur, independent of how the star (or model) got there. Plausible calculations and their dynamical outcomes that seem to reproduce observations of Type Ia supernovae (Höflich, Nomoto, Umeda & Wheeler 2000; Dominguez, Höflich & Straniero 2001) give ignition densities of about $1.5 - 2.5 \times 10^9 \text{ gm cm}^{-3}$, right where the Ne/Na convective Urca “on” switch might lie. This means that whether a model (and hence a real star, in principle) does or does not trigger the convective Urca process with its potential effect on convective velocity fields, extent of convection, amount of carbon burning between ignition and runaway, and the C/O gradient at runaway, may depend sensitively on such recently neglected issues as electron screening and plasmon neutrino loss rates. We also note that the white dwarfs that explode as Type Ia supernovae will almost surely be rotating. The rotational state will also affect the carbon ignition density (Piersanti et al.

2003a,b) and hence the presence of convective Urca effects.

Another important issue is the abundance of a given Urca-active pair. We have shown that the kinetic energy of convective motion is rather independent of the abundance of the Urca nuclei, but that the mixing of carbon and its burning products does depend on the Urca abundance. We also find that neutrino losses are reduced (within the range of parameters explored here) for higher abundance of Urca nuclei, although we cannot rule out that this is an effect of our numerical resolution. The abundance of Urca-active nuclei are a function explosive nucleosynthesis in prior generations of stars and so the role of the convective Urca process might be a function of redshift. Another possible effect on abundances is evolution in the core. If burning prior to runaway should produce more Urca nuclei, then the Urca process could be enhanced.

Other interesting issues are related to the location of the Urca shell (or shells) and the speed of convection. How does the Urca process work if the central density is only slightly above the Urca threshold so that the Urca shell is quite small, smaller, perhaps, than a convective scale length? In general, how fast is the convection? Sufficiently rapid convection will sweep mothers back down to regions where they are stable before they can decay. We note that when carbon ignition first occurs, the convection is likely to start slowly, giving the Urca process ample time to work, as long as the ignition density exceeds the Urca threshold.

The key question is, even if there is an active convective Urca stage in the evolution toward dynamic runaway, does this make any substantial difference in the nature of that runaway and the subsequent dynamics? If the Urca process limits the radial extent of the convection, somewhat more carbon might be consumed within the Urca shell than beyond. On the other hand, the total amount of carbon consumed is likely to be small and if the limitation on the extent of convection breaks down before dynamic runaway, then there will be a homogenization process as the convection sweeps outward and dredges carbon inward. It seems unlikely that an effect of the convective Urca process on the abundance, *per se*, will be significant.

A potentially more interesting effect is on the velocity structure of the convective motion. Höflich & Stein (2002) investigated the final 3 hours before dynamic runaway with implicit two-dimensional calculations. They showed that the “smoldering” phase of nuclear burning that immediately precedes dynamical runaway can produce convective motions with velocities of order $40 - 120 \text{ km s}^{-1}$. There were two implications of this work. One was that dynamical runaway was triggered at a single region near to, but definitely away from, the center of the star by compression driven by converging convective plumes. The second implication was that the convective speeds were comparable to, or even exceeded, the velocity of the burning front in the early, slow, phase of Rayleigh-Taylor unstable turbulent deflagra-

tion. This means that the convective velocity field can substantially “prepare” the conditions prior to dynamical runaway, can trigger the dynamical runaway, and that in the early phases of dynamical runaway it is still the convective velocities, not the burning front velocity, that determine the speed of propagation of the burning front. Recent calculations by Kuhlen et al. (2005) have addressed aspects of the late smoldering phase in three-dimensional calculations. They have not followed the burning completely to dynamic runaway, but find qualitatively similar results over the limited time frame they investigated: convective flows of order $50 - 130 \text{ km s}^{-1}$ and hot spots near the center where dynamic runaway might occur. The outcome of dynamical ignition may depend sensitively on the number and location of the runaway spots leading in some cases to single plumes of burning and in others to more homogeneous outward propagation of the early deflagration burning (Livne, Asida & Höflich 2005).

The convective Urca process could thus affect the nature of the convective velocity field and hence the smoldering phase, the location of dynamic runaway, and the early stages of dynamical runaway. The current calculations allow us to raise such issues, but because of the artificial speed up of the nuclear and weak interaction rates, we cannot address them directly here. The speed up of the nuclear rates by a factor of 20,000 will result in a speedup of the convective velocities. In the current models, the convective motions are of order 10 km s^{-1} . The question is what happens in a realistic model. Will the presence of the convective Urca shell continue to confine the convection and will the convective velocities in the smoldering phase that precedes dynamical runaway be restricted and hence less able to affect the early stages of deflagration? Or will the convection speed up and somehow “break out” of the Urca shell yielding results similar to those of Höflich & Stein (2002) who neglected the convective Urca process.

In this context, the important issue is whether the convection becomes strong enough within an active Urca zone to overwhelm the Urca control and thus spread the convection throughout its “natural” regime as if there were no Urca processes. The convective Urca process might control the extent of the convection through much of the smoldering phase only to be overwhelmed in the final few hours or minutes before dynamic runaway; sufficient time to establish a convective structure that lost all memory of the convective Urca phase.

That this breakdown of the convective Urca process could occur can be seen qualitatively by considering that for sufficiently strong convection, convective flows may push substantially beyond the Urca shell to the point where all the mothers have decayed to daughters and there will be no more neutrino losses regardless of how far the convection thus extends. We have shown in Figures 1 and 2 that the convective kinetic energy and neutrino loss rates increases with the nuclear reaction rates, but, at least for these simulations, at a rate that is

slower than linear. These simulations also suggest that within the range we have explored, the neutrino loss rates scale roughly linearly with the convective energy. These conclusions hold as long as the Urca shell can control the convection. We sketch in the Appendix an argument that suggests that sufficiently strong convection can cause the convection to “break out” and overwhelm the limits of the convective Urca process. In principle, our use of accelerated nuclear reaction rates might correspond to a later phase in the smoldering process, closer to dynamical runaway, although it is not clear this is true. Based on our simulations, we estimate in the Appendix that convective velocities substantially in excess of 20 to 70 km s⁻¹, depending on the abundance of the Urca-active nuclei, are required for “breakout.” Interestingly, this is similar to the velocity range found in the studies of Höflich & Stein (2002) and of Kuhlen et al. (2005) for the late smoldering phase. This suggests that breakout might, or might not, occur prior to dynamical runaway. We conclude that this issue is open and in need of thorough future study. While there is no obvious reason to think the convective Urca process will affect subsequent dynamic phases, we currently have no grounds to rule out that it may do so.

Although the convective Urca process has been long neglected, the current calculations suggest that it needs to be in the suite of actively-considered physical phenomena as we attempt to achieve a refined level of understanding of Type Ia supernovae. We have identified a number of important issues regarding the convective Urca process that need to be explored in multidimensional calculations that investigate the evolution from carbon ignition to dynamical runaway. A key issue is the behavior of the convective Urca process without the artificial enhancement in rates we have employed and in three dimensions.

We are grateful to Peter Höflich for discussion of related topics of degenerate convective carbon burning. This research was supported in part by NSF Grant AST-0098644,

A. An Estimate of Urca Stopping Power

In order to get a rough estimate of the stopping power of the Urca effect, let us assume that one blob of unit mass of material containing concentration of mothers, X_m , crosses the Urca-shell outward. its velocity \mathbf{u} is perpendicular to the Urca-shell. Let us further assume that the Urca effect is local, i.e., when mothers become daughters in the blob, the blob loses kinetic energy equivalent to the neutrino + heat energy released in the process. This estimate would be straight forward except that the energy lost depends on the location in which it was released: the further from the Urca-shell, the more energy is lost to neutrinos plus β -decay heating.

Let x be the distance of the blob from the Urca-shell, then, under the above assumptions, the motion of the blob is governed by the following equations:

$$\frac{dx}{dt} = \mathbf{u} \quad (\text{A1})$$

$$\frac{dX_m}{dt} = -C_\nu \eta^3 x^3 X_m \quad (\text{A2})$$

where $C_\nu \eta^3 x^3$ is the rate of capture per atom with C_ν being a numerical coefficient (units $\text{erg}^{-3} \text{ s}^{-1}$) characteristic of a given Urca pair, $\eta = |\frac{dE_F}{dx}|$, at $x = 0$, N_A is Avogadro's number and A is the atomic number of the Urca atoms.

If the blob is not stopped by the Urca process, but loses a fraction of its kinetic energy, then X_m goes to 0 for large x where all β -decay has gone to completion. Then $|\frac{dX_m}{dt}|$ has a maximum at some point x_c . Let us assume that the whole reaction occurs near that point. At the maximum we have: $x_c = (\frac{3u}{C_\nu \eta^3})^{\frac{1}{4}}$. The energy released at the maximum is:

$$E_c = \frac{N_A}{A} X_m \eta x_c = \frac{N_A}{A} X_m \eta \times \left(\frac{3u}{C_\nu \eta^3}\right)^{\frac{1}{4}} = \frac{N_A}{A} X_m \left(\frac{3u \eta}{C_\nu}\right)^{\frac{1}{4}}. \quad (\text{A3})$$

Therefore, in order to continue moving outward, the blob should have kinetic energy significantly larger than E_c , or

$$u > \left(\frac{N_A}{A} X_m\right)^{\frac{1}{2}} \left(\frac{48u \eta}{C_\nu}\right)^{\frac{1}{8}} \quad (\text{A4})$$

or

$$u > \left(\frac{48\eta}{C_\nu} \left(\frac{N_A}{A} X_m\right)^4\right)^{\frac{1}{7}}. \quad (\text{A5})$$

Note that this criterion depends only weakly on the Urca rate and is only mildly sensitive to the Urca abundance.

In our case $\nu = 2000 \times 3.3 \times 10^{13} = 6.6 \times 10^{16} \text{ erg}^{-3} \text{ s}^{-1}$ (Ergma & Paczyński 1974), $\eta = 0.86 \times 10^{-13}$, and $A = 23$, so when $X_m = 4 \times 10^{-4}$ then u must be significantly greater than 70 km s^{-1} . When $X_m = 4 \times 10^{-5}$, u must be significantly greater than 19 km s^{-1} .

REFERENCES

Barkat, Z. & Wheeler, J. C. 1990, *ApJ*, 355, 602

Bisnovatyi-Kogan, G. S. 2001, *MNRAS*, 321, 315

Bisnovatyi-Kogan, G. S. & Seidov, Z. F. 1970, *Astron. Zh.* 47, 139

Brachwitz, F. et al. 2000, *ApJ*, 536, 934

Bravo, E. et al. 1996, *A&A*, 306, 811

Bruenn, S. W. 1973, *ApJ*, 183, L125

Couch, R. G. & Arnett, W. D. 1975, *ApJ*, 196, 791

Domínguez, I., Höflich, P., & Straniero, O. 2001, *ApJ*, 557, 279

Ergma, E. & Paczyński, B. E. 1974, *Acta Astron.* 24, 1

Finzi, A. & Wolf, R. A. 1968, *ApJ* 153, 835

Höflich, P. & Stein, Y. 2002, *ApJ*, 568, 779

Iben, I. I., Jr. 1978a, *ApJ*, 219, 213

Iben, I. I., Jr. 1978b, *ApJ*, 226, 996

Iben, I. I., Jr. 1982, *ApJ*, 253, 248

Itoh, I. & Kohyama, Y. 1983, *ApJ*, 275, 858

Kuhlen, M., Woosely, S. E. & Glatzmaier, G. A. *ApJ*, submitted (astro-ph/0509367)

Lesaffre, P., Podsiadlowski, Ph. & Tout, C. A. 2005, *MNRAS*, 356, 131

Lesaffre, P., Han, Z., Tout, C. A., Podsiadlowski, Ph. & Martin, R. G. 2006, *MNRAS*, submitted

Livne, E., 1993, *ApJ*, 412, 634

Livne, E., Asida, S. M. & Höflich, P. 2005, *ApJ*, in press (astro-ph/0504299)

Mochkovitch, R. 1996, *A&A* 311, 152

Paczyński, B. E. 1972, *Astrophys. Lett.*, 11, 53

Paczyński, B. E. 1974, *Astrophys. Lett.*, 15, 147

Piersante, L. et al. 2003a, *ApJ*, 583, 885

Piersante, L. et al. 2003b, *ApJ*, 598, 1229

Stein, J., Barkat, Z. & Wheeler, J. C. 1999, *ApJ*, 523, 381

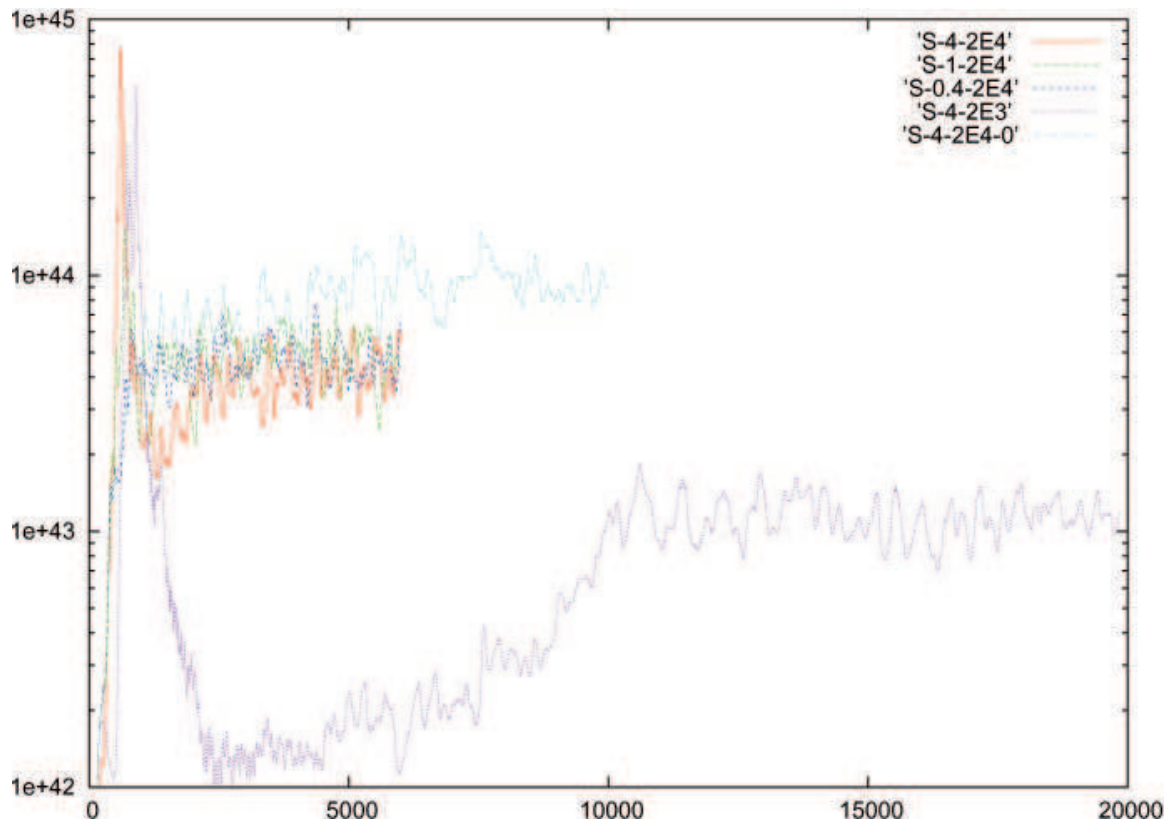


Fig. 1.— Plot of convective kinetic energy versus simulation time, for simulations S-4-2E4, S-1-2E4, S-0.4-2E4, S-4-2E3, and S-4-2E4-0. Simulations S-4-2E4, S-1-2E4, S-0.4-2E4, and S-4-2E4-0 had the nuclear rates multiplied by 2×10^4 and simulation S-4-2E3, had the nuclear rate multiplied by 2×10^3 .

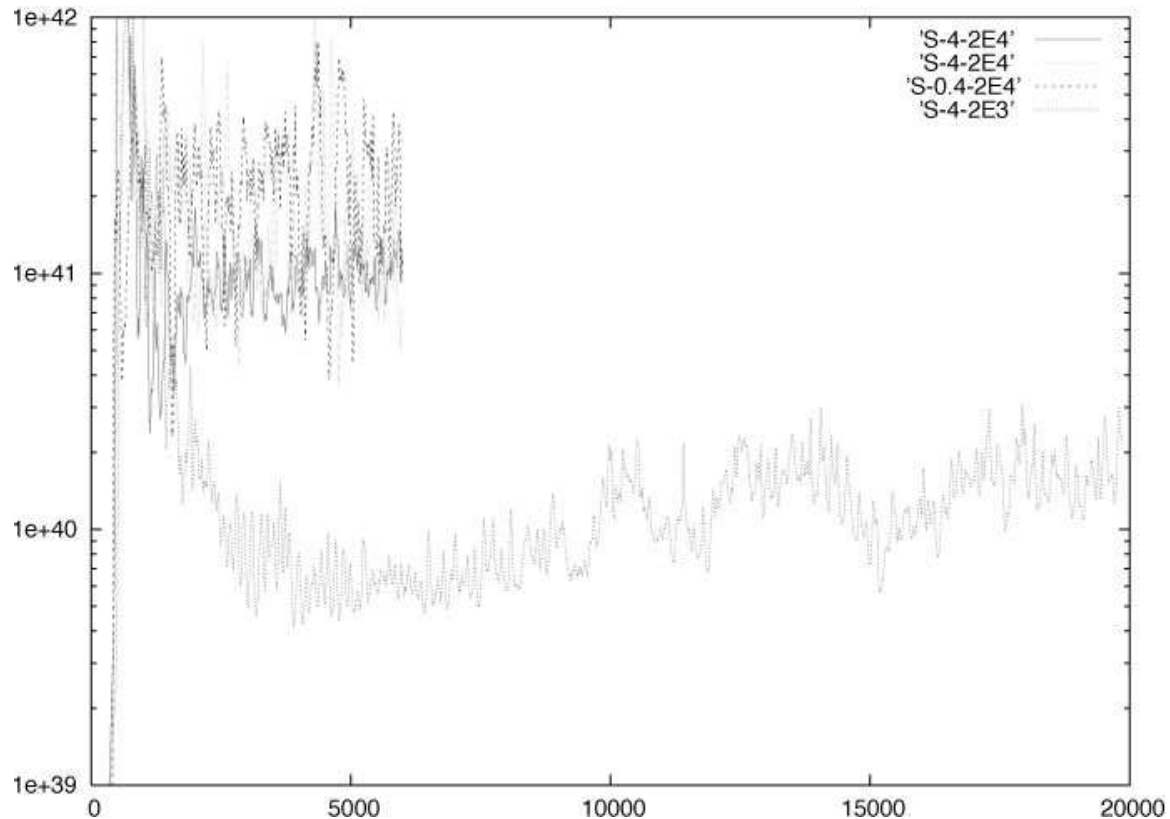


Fig. 2.— Plot of Urca neutrino loss versus simulation time, of simulations S-4-2E4, S-1-2E4, S-0.4-2E4 and S-4-2E3. Simulations S-4-2E4, S-1-2E4, S-0.4-2E4 had the nuclear rate multiplied by 2×10^4 and simulation S-4-2E3 had the nuclear rate multiplied by 2×10^3 .

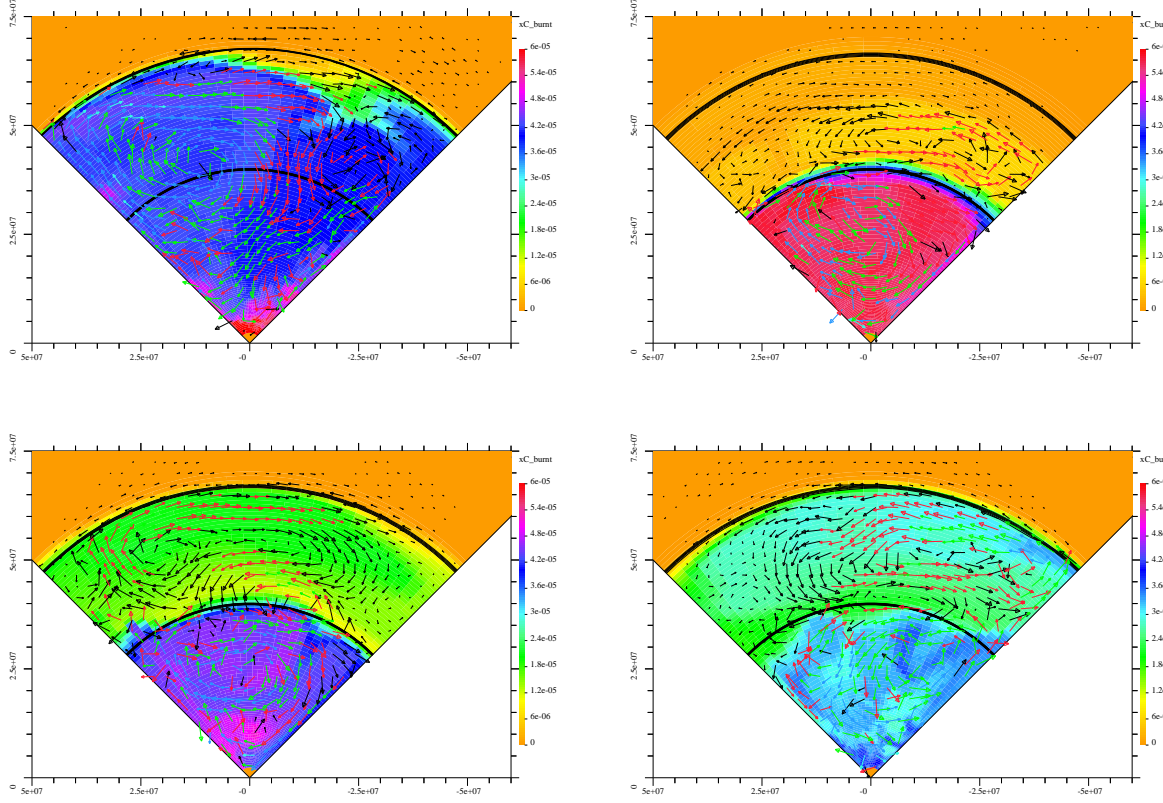


Fig. 3.— A) (upper left) Plot of the distribution of carbon-burning products, velocity vectors, the Urca shell (heavy black line around $R = 400$ Km) and the boundary separating the inner region of constant entropy from the outer isothermal region (thinner black line around 670 Km) for simulation S-4-2E4-0 with no Urca process. The carbon-burning products are distributed more or less evenly in the whole inner region. B) (upper right) Same as A but for simulation S-4-2E4 with the Urca process turned on. The carbon-burning products are almost entirely confined to the inner zone (within the Urca-shell). Strong convection is seen in the inner zone, and a separate convection region exists in the outer zone between the Urca shell and the boundary of the isothermal region, probably triggered by the overshoot from the inner zone. C) (lower left) same as B) but for simulation S-1-2E4 with smaller abundance of Urca-active nuclei. The carbon-burning products are less confined to the inner zone (within the Urca-shell) than in B. The velocities near the Urca-shell are almost parallel to the shell. D) (lower right) Same as B and C but for simulation S-0.4-2E4 with even smaller abundance of Urca-active nuclei. The carbon-burning products are less confined to the inner zone (within the Urca-shell) than in C. Velocity vectors are normalized such that one horizontal tic mark represents 10 km s^{-1} (journal black and white version) or black arrows: less than 1 km s^{-1} ; red arrows: $1 - 2 \text{ km s}^{-1}$; green arrows: $2 - 4 \text{ km s}^{-1}$; blue arrows: $4 - 8 \text{ km s}^{-1}$ (on-line color version).

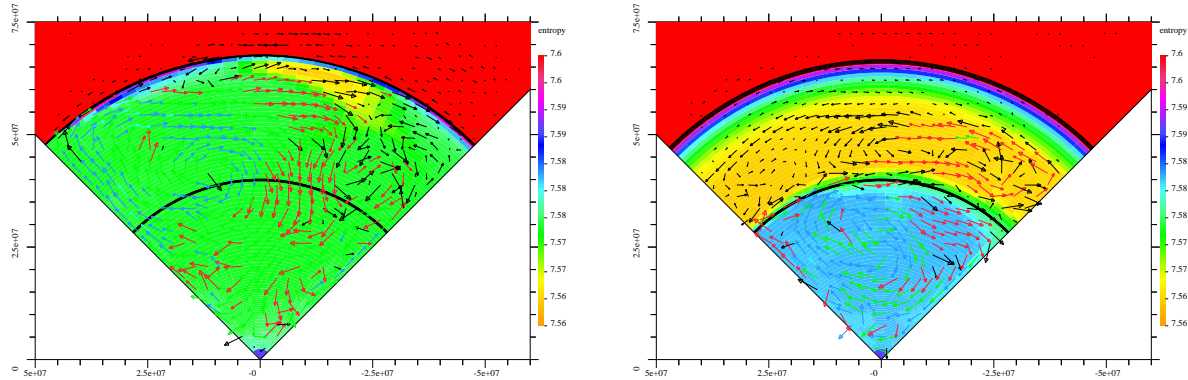


Fig. 4.— A) (left panel) Plot of entropy, velocity vectors, Urca shell as in Figure 3 at 10,000 seconds for simulation S-4-2E4-0 with no Urca effect. B) (right panel) same as A, but with Urca effect and time = 6000 sec for simulation S-4-2E4.

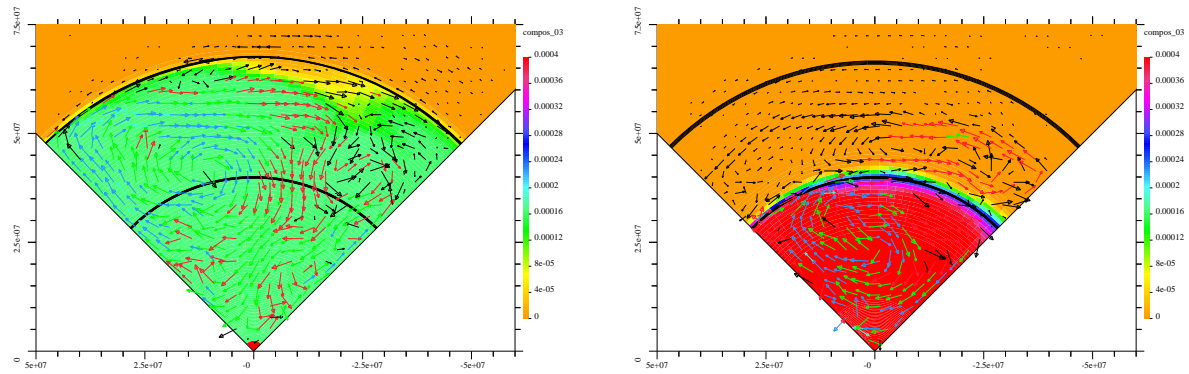


Fig. 5.— A) (left panel) Plot of Ne^{23}/Na^{23} abundance, velocity vectors, Urca shell as in Figure 3 at 10,000 seconds for simulation S-4-2E4-0 with no Urca effect. B) (right panel) same as A, but with Urca effect and time = 6000 sec for simulation S-4-2E4.

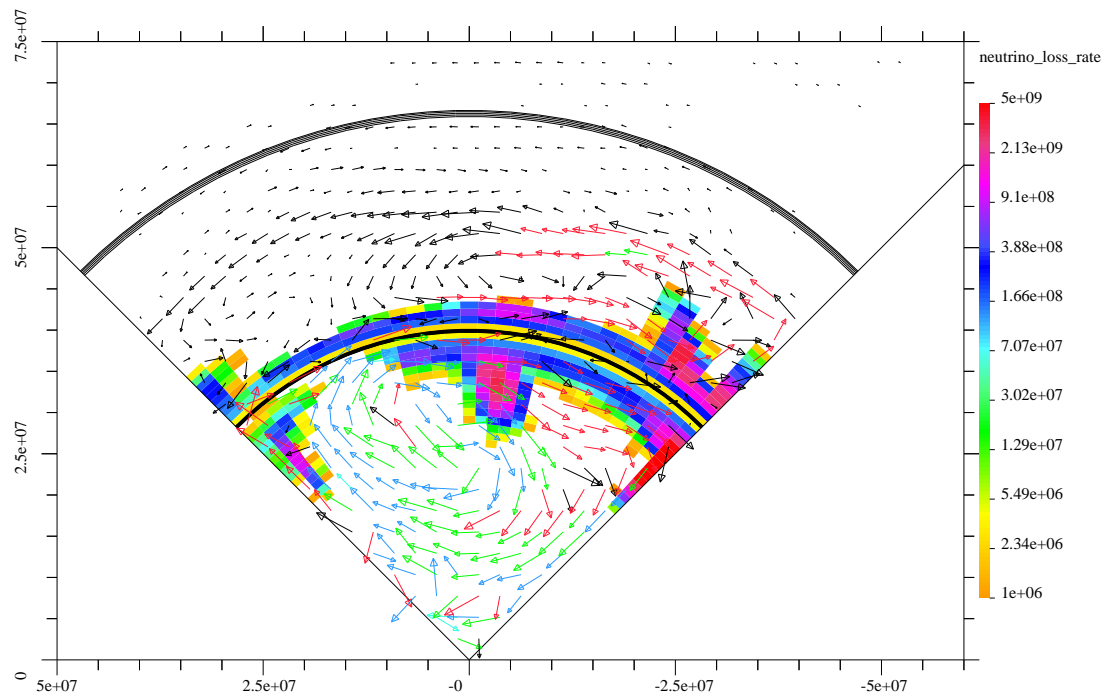


Fig. 6.— Plot of Urca neutrino loss for simulation S-4-2E4. The whole Urca activity occurs near the Urca-shell. Areas adjacent to the left and right boundaries are subject to numerical artifacts and should be ignored. Velocity vectors are represented as in Figure 3.